RESEARCH BRIEF

The Genetic Basis of Hepatosplenic T-cell Lymphoma

Matthew McKinney[1], Andrea B. Moffitt[2], Philippe Gaulard[3], Marion Travert[3], Laurence De Leval[4], Alina Nicolae[5], Mark Raffeld[5], Elaine S. Jaffe[5], Stefania Pittaluga[5], Liqiang Xi[5], Tayla Heavican[6], Javeed Iqbal[6], Karim Belhadj[3], Marie Helene Delfau-Larue[3], Virginie Fataccioli[3], Magdalena B. Czader[7], Izidore S. Lossos[8], Jennifer R. Chapman-Fredricks[8], Kristy L. Richards[9], Yuri Fedoriw[9], Sarah L. Ondrejka[10], Eric D. Hsi[10], Lawrence Low[11], Dennis Weisenburger[11], Wing C. Chan[11], Neha Mehta-Shah[12], Steven Horwitz[12], Leon Bernal-Mizrachi[13], Christopher R. Flowers[13], Anne W. Beaven[1], Mayur Parihar[14], Lucile Baseggio[15], Marie Parrens[16], Anne Moreau[17], Pierre Sujobert[18], Monika Pilichowska[19], Andrew M. Evens[19], Amy Chadburn[20], Rex K.H. Au-Yeung[21], Gopesh Srivastava[21], William W. L. Choi[21], John R. Goodlad[22], Igor Aurer[23], Sandra Basic-Kinda[23], Randy D. Gascoyne[24], Nicholas S. Davis[1], Guojie Li[1], Jenny Zhang[1], Deepthi Rajagopalan[1], Anupama Reddy[1], Cassandra Love[1], Shawn Levy[25], Yuan Zhuang[1], Jyotishka Datta[26], David B. Dunson[26], and Sandeep S. Davé[1,2]

ABSTRACT

Hepatosplenic T-cell lymphoma (HSTL) is a rare and lethal lymphoma; the genetic drivers of this disease are unknown. Through whole-exome sequencing of 68 HSTLs, we define recurrently mutated driver genes and copy-number alterations in the disease. Chromatin-modifying genes, including *SETD2, INO80,* and *ARID1B,* were commonly mutated in HSTL, affecting 62% of cases. HSTLs manifest frequent mutations in *STAT5B* (31%), *STAT3* (9%), and *PIK3CD* (9%), for which there currently exist potential targeted therapies. In addition, we noted less frequent events in *EZH2, KRAS*, and *TP53*. *SETD2* was the most frequently silenced gene in HSTL. We experimentally demonstrated that *SETD2* acts as a tumor suppressor gene. In addition, we found that mutations in *STAT5B* and *PIK3CD* activate critical signaling pathways important to cell survival in HSTL. Our work thus defines the genetic landscape of HSTL and implicates gene mutations linked to HSTL pathogenesis and potential treatment targets.

SIGNIFICANCE: We report the first systematic application of whole-exome sequencing to define the genetic basis of HSTL, a rare but lethal disease. Our work defines *SETD2* as a tumor suppressor gene in HSTL and implicates genes including *INO80* and *PIK3CD* in the disease. *Cancer Discov; 7(4); 369–79. ©2017 AACR.*

See related commentary by Yoshida and Weinstock, p. 352.

[1]Duke Cancer Institute, Duke University Medical Center, Durham, North Carolina. [2]Duke Center for Genomics and Computational Biology, Duke University, Durham, North Carolina. [3]Hôpital Henri Mondor, Department of Pathology, AP-HP, Créteil, France, INSERM U955, Créteil, France, and University Paris-Est, Créteil, France. [4]Pathology Institute, CHUV Lausanne, Switzerland. [5]Laboratory of Pathology, National Cancer Institute, National Institutes of Health, Bethesda, Maryland. [6]University of Nebraska, Omaha, Nebraska. [7]Indiana University, Indianapolis, Indiana. [8]University of Miami, Miami, Florida. [9]University of North Carolina, Chapel Hill, North Carolina. [10]Cleveland Clinic, Cleveland, Ohio. [11]City of Hope Medical Center, Duarte, California. [12]Memorial Sloan Kettering Cancer Center, New York, New York. [13]Emory University, Atlanta, Georgia. [14]Tata Medical Center, Kolkata, India. [15]Centre Lyon-Sud, Pierre-Bénite, France. [16]Hôpital Pessac, Bordeaux, France. [17]Pathology, Hôpital Hôtel-Dieu, Nantes, France. [18]Faculté de Médecine Lyon-Sud Charles Mérieux, Université Claude Bernard, Lyon, France. [19]Tufts University Medical Center, Boston, Massachusetts. [20]Presbyterian Hospital, Pathology and Cell Biology, Cornell University, New York, New York. [21]University of Hong Kong, Queen Mary Hospital, Hong Kong, China. [22]Department of Pathology, Western General Hospital, Edinburgh, UK. [23]University Hospital Centre Zagreb, Zagreb, Croatia. [24]British Columbia Cancer Agency, University of British Columbia, Vancouver, Canada. [25]Hudson Alpha Institute for Biotechnology, Huntsville, Alabama. [26]Department of Statistical Science, Duke University, Durham, North Carolina.

Note: Supplementary data for this article are available at Cancer Discovery Online (http://cancerdiscovery.aacrjournals.org/).

M. McKinney and A.B. Moffitt contributed equally to this article.

Corresponding Author: Sandeep S. Davé, 101 Science Drive, Duke University, Durham, NC 27710. Phone: 919-681-1922; Fax: 919-681-1777; E-mail: ssd9@duke.edu

doi: 10.1158/2159-8290.CD-16-0330

INTRODUCTION

Hepatosplenic T-cell lymphoma (HSTL) is a rare type of peripheral T-cell lymphoma (PTCL) that affects fewer than 2% of all patients with lymphoma each year. Compared with other PTCL subtypes, HSTL is striking for its predilection for young individuals and its dismal prognosis; most patients with HSTL succumb to their disease in less than a year (1, 2).

Although the vast majority of PTCLs arise from αβ T cells, HSTL arises predominantly (>80%) from γδ T cells. Immunosuppression is a major risk factor for HSTL, particularly in the setting of organ transplantation and exposure to thiopurines or TNFα antagonists, but most HSTL cases arise sporadically in the absence of any known factors. Most patients with HSTL are treated with combination chemotherapy and, when feasible, bone marrow transplantation, but relapses are frequent and the overwhelming majority of patients succumb to HSTL.

The most frequent known genetic abnormalities in HSTL are isochromosome 7q (iso7q; refs. 3, 4) and trisomy 8 (5, 6), but the role of somatic mutations and other genomic alterations in HSTL has yet to be defined. Application of next-generation sequencing in other PTCLs (7–18) has revealed a strikingly heterogeneous genetic landscape implicating over a dozen different genetic alterations, including therapeutic targets. Similar systematic studies in HSTLs have been lacking.

In this study, we sought to define the genetic landscape of HSTL through whole-exome sequencing of 68 HSTL cases, including 20 cases with paired germline DNA. We found that HSTLs have a distinct pattern of genetic alterations. In addition to iso7q and trisomy 8, HSTLs manifested frequent mutations in the genes *SETD2, INO80, STAT5B, SMARCA2, TET3,* and *PIK3CD*. Interestingly, mutations that occur frequently in other T-cell lymphomas in genes such as *RHOA, CD28*, and *CCR4* were notably absent or occurred at much lower frequency in HSTLs. Finally, through functional studies in HSTL cells, we demonstrated *SETD2* to be a tumor suppressor gene that mediates increased cellular proliferation in HSTL. In addition, we found that mutations in *STAT5B* and *PIK3CD* activate critical signaling pathways important to cell survival in HSTL.

To our knowledge, this study is the largest series of patients with HSTL ever described and defines in detail the genetic landscape of mutations, implicating a number of genes and molecular pathways in this disorder.

RESULTS

Whole-Exome Sequencing of HSTL Identifies Gene Coding Mutations and Chromosomal Copy-Number Alterations

We performed whole-exome sequencing on 68 primary HSTL tumors, 20 with paired normal tissue, and 2 HSTL cell lines (i.e., total 90 exomes). The bioinformatics methods are described more comprehensively in the Supplementary Methods. The 20 cases with paired normal tissue were deemed a "discovery set," and the remaining samples a "validation set." Only genes found to be somatically mutated in the discovery set were initially considered as candidate driver genes in HSTL.

As expected, patients with HSTL in our study had a dismal prognosis, with a median survival of 11.9 months following diagnosis. The majority (63%) of the patients died within 2 years of diagnosis (Fig. 1A). HSTL driver genes are depicted as a heat map in Fig. 1B. The distribution of alterations of these genes in the different HSTL cases is shown in Fig. 1B, and the frequency of these events is shown in Fig. 1C. Chromatin-modifying genes constituted the most frequently mutated group of genes in HSTL, accounting for 62% of the cases. *SETD2* was the most commonly mutated chromatin-modifying gene in HSTL (24 mutations found in 17 patients) with 71% (12/17) of the cases manifesting at least one loss-of-function (nonsense or frameshift) mutation. *SETD2* showed strong selection for protein-altering mutations, with only one synonymous mutation observed. Other frequently mutated chromatin modifier genes included *INO80* (21%), *TET3* (15%), and *SMARCA2* (10%). Mutations in signaling pathways comprised the next most common group of mutations and manifested as predominantly missense mutations in *STAT5B, STAT3*, and *PIK3CD*. In addition, we observed mutations in *TP53, UBR5*, and *IDH2*. Among these gene mutations, only those in *STAT5B* and *STAT3* have been described in HSTLs previously (19, 20). We verified the accuracy of genetic variant identification from our deep-sequencing data by performing Sanger sequencing in 78 individual variant events from the same cases (Supplementary Table S1). Representative plots from Sanger validation are shown in Supplementary Fig. S1a–S1b. We found that Sanger sequencing agreed with our methods in 88% of the variants, confirming that our laboratory methods for deep sequencing and computational methods for identifying genetic variants generated accurate results. We identified 13 somatically mutated HSTL driver genes (Supplementary Table S2) using a model that relies on the frequencies of nonsynonymous events in HSTL, the size of the gene, the rate of nonsynonymous variation occurring in the gene in healthy controls, and the predicted impact of the altered amino acid(s) as we have described previously (21–23).

Estimates of cancer cell fraction based on observed allele frequencies for each driver gene are shown in Supplementary Fig. S2a. *STAT3, PIK3CD*, and *SETD2* show the highest proportion of clonal events among the driver genes. We compared cancer cell fractions (allele frequency adjusted for tumor purity) for pairs of mutations occurring in the same sample (Supplementary Fig. S2b) and found considerable heterogeneity in the genes that arose as predominant drivers in different cases. In addition, we examined mutation data for the presence of well-characterized driver mutations, even in the absence of a clear somatic event in the discovery set. We identified rare mutations in a number of known driver genes, including *KRAS* ($N = 3$) and *CREBBP* ($N = 2$), that have been described in other cancers. Additional somatic mutations found and putative driver mutations are shown in Supplementary Table S3.

We further examined chromosomal alterations in HSTLs (Fig. 1D). Alterations in chromosome 7 were the most common genetic abnormality in HSTLs, affecting 47% (Supplementary Table S4; Supplementary Fig. S3) of our cases. Although the majority of cases manifested clearly as iso7q with losses of chromosome 7p and gains of 7q, there were five cases

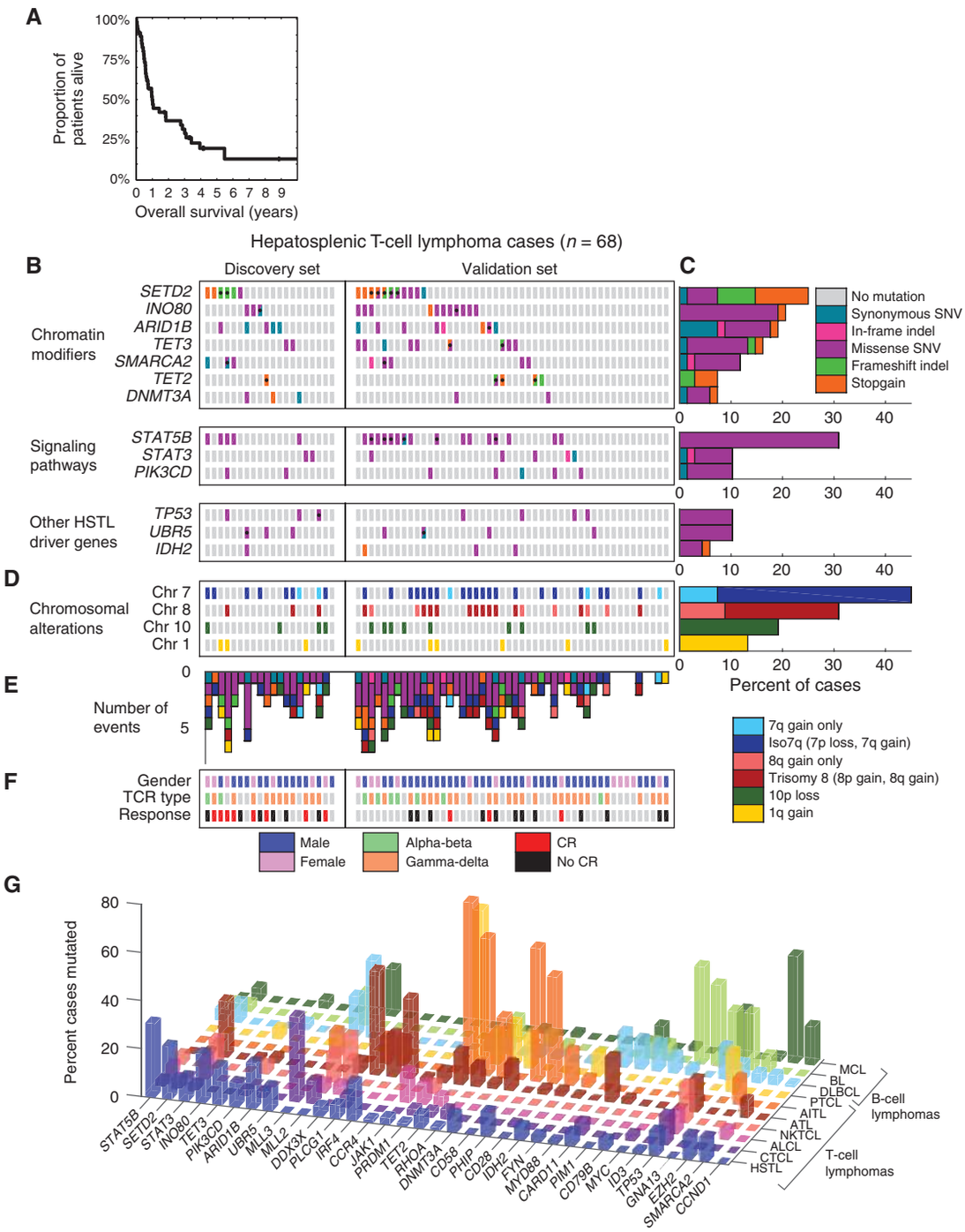

Figure 1. Characterization of mutations, copy number, clinical data, and survival in HSTL cases. **A,** Kaplan–Meier curve for all HSTL cases with available survival data ($n = 47$). Median survival is 11.9 months. Median follow-up is 4.2 years. **B,** Heat map of mutated genes in HSTL ($n = 68$). Each row represents a mutated gene in HSTL. Each column represents a patient sample. Blocks are color-coded by functional type of mutation (orange, stopgain SNV; green, frameshift indel; purple, missense SNV; pink, nonframeshift indel; teal, synonymous). Samples are separated into discovery set ($n = 20$) with paired normal and validation set ($n = 48$). Samples with more than one variant per gene are indicated with black dots on the block. **C,** Number of cases affected per gene. Bars colored by most damaging mutation in each gene–sample pair. **D,** Copy-number alterations of chromosomes 7p and 7q, 8p and 8q, 10p, and 1q (light blue/dark blue: chromosome 7, light red/dark red: chromosome 8, dark green: chromosome 10p, yellow: chromosome 1q). **E,** Number of events per sample, including significant mutations and arm-level copy-number changes. **F,** Heat map of clinical variables: gender (blue, male; pink, female), T-cell receptor (TCR) type (light green, alpha-beta; light orange, gamma-delta), and response to initial treatment [red: complete response (CR); black, no CR]. **G,** Mutation frequency (vertical bars) of genes in HSTL ($N = 68$), blue; cutaneous T-cell lymphoma (CTCL; $N = 37$), dark purple; anaplastic large cell lymphoma (ALCL; $N = 23$), magenta; natural killer/T-cell lymphoma (NKTCL; $N = 25$), pink; adult T-cell leukemia/lymphoma (ATL; $N = 81$), red; angioimmunoblastic T-cell lymphoma (AITL; $N = 28$ or 9), orange; peripheral T-cell lymphoma (PTCL; $N = 22$ or 6), yellow; diffuse large B-cell lymphoma (DLBCL; $N = 96$), light blue; Burkitt lymphoma (BL; $N = 59$), light green; and mantle cell lymphoma (MCL; $N = 56$), dark green.

with only 7q amplifications. Supplementary Fig. S3 shows the exact regions of chromosome 7 altered in all the affected cases, which are complete arm-level alterations in the vast majority of cases. Trisomy 8 or amplifications of 8q was the next most frequent chromosomal aberration (31%), frequently co-occurring with chromosome 7 alterations (18 overlapping cases). We also found that losses in chromosome 10q (19%) and gains in chromosome 1q (13%) occurred in a significant proportion of HSTL cases. The only driver gene that is located within these copy-number regions is *UBR5*, on chromosome 8q. We did not find any mutations that clearly overlapped or occurred independently of these chromosomal alterations. The median number of genetic alterations per sample in these driver mutation and copy-number events was three (Fig. 1E).

We also sequenced the only described HSTL cell lines, DERL2 and DERL7, which are derived from the same primary HSTL tumor (24). Their genetic profiles were nearly identical, and representative of the HSTL tumors, with mutations in *STAT5B, ARID1B, SMARCA2*, and *TP53*, as well as copy-number alterations of isochromosome 7q, trisomy 8, loss of 10p, and gain of 1q (Supplementary Fig. S4a–S4b).

Clinical Characteristics of Patients with HSTL

The patients' gender, T-cell receptor type, and response to initial therapy are shown for comparison with the molecular features in Fig. 1F. The clinical characteristics of our patients are summarized in Table 1.

Briefly, the median age was 42 (range, 4–72). As expected, male patients comprised the majority (71%) of the cohort, with a worse prognosis than females ($P = 0.05$, log-rank test). Elevated lactate dehydrogenase (LDH) levels and Eastern Cooperative Oncology Group (ECOG) performance status ($P = 0.002$ for both, log-rank test) were the clinical variables most clearly associated with outcome. Eighty percent of cases

Table 1. Summary of clinical variables and survival association

Clinical feature	Clinical/pathological characteristic	Number of cases (%)	Log-rank univariate test for survival association *P* value
Age	Median (years)	42	NS
	0–35 years	23 (42)	
	35–50 years	16 (30)	
	>50 years	15 (28)	
Gender	Male	48 (71)	0.054
	Female	20 (29)	
Race	Caucasian	50 (74)	NS
	African	13 (19)	
	Asian	4 (6)	
	Hispanic	1 (1)	
ECOG performance status	0–1	21 (62)	0.002
	2–4	13 (38)	
LDH level	Elevated	24 (67)	0.002
TCR type	Gamma-delta	37 (80)	NS
	Alpha-beta	9 (20)	
Chr 7 aberration	Present	33 (49)	0.051
	Absent	35 (51)	
Chr 8 aberration	Present	21 (31)	0.024
	Absent	47 (70)	
Treatment	Chemotherapy only	37 (93)	—
	Autologous or allogenic transplant	10 (26)	0.014
Response to initial treatment	CR	11 (38)	0.001 (CR vs. non-CR)
	PR/SD	7 (24)	
	NR/PD	11 (38)	
Survival	Median survival (months)	11.9	—
	Median follow-up (months)	49.8	
	Alive at 6 months	35 (75)	
	Alive at 12 months	24 (50)	
	Alive at 24 months	17 (37)	

NOTE: Clinical characteristics, the most common copy-number aberrations, treatment, and outcome statistics for the cohort are summarized. The number of cases with each feature are listed, as well as a percentage of the cohort, excluding samples with missing data for that variable. Association with survival is tested with a univariate log-rank test, and *P* values are provided for the significant tests ($P < 0.1$).

Abbreviations: CR, complete response; NR, no response; NS, not significant; PD, progressive disease; PR, partial response; SD, stable disease; TCR, T-cell receptor.

were of the γδ T-cell receptor (TCR) type, but no survival association was seen with the TCR type. Patients with a complete response (CR) to initial treatment and those patients who received an autologous or allogenic transplant following initial treatment had significantly improved outcomes ($P = 0.001$ and 0.014, respectively). Supplementary Table S5 contains complete clinicopathologic data, and Supplementary Fig. S5 shows the Kaplan–Meier plots for these and additional clinical variables.

We also investigated the association of genetic mutations and copy-number alterations with clinical outcome in an exploratory fashion. The most robust survival associations within the genetic features were found with the copy-number alterations on chromosomes 7 and 8 ($P = 0.051$ and 0.024, respectively), which were both associated with worse outcomes. Kaplan–Meier plots for these molecular covariates are shown in Supplementary Fig. S6. Additional survival analyses are presented in the Supplementary Methods.

These data add clarity to other studies that have postulated links between clinicopathologic or molecular features and patient-level outcomes in HSTL (Supplementary Table S6). Supplementary Table S7 shows the similarity of our patient cohort to those previously reported.

Genetic Differences between HSTL and Other T-cell and B-cell Lymphomas

HSTL has a distinct clinical presentation and response to therapy compared with other B- and T-cell lymphomas. We next investigated whether HSTLs are also genetically distinct from these tumors. We compared the frequencies of the most recurrently mutated genes in HSTL to other lymphomas studied by whole-exome sequencing, including the T-cell lymphomas PTCL not otherwise specified (PTCL NOS; ref. 8), angioimmunoblastic T-cell lymphoma (AITL; refs. 8, 12), cutaneous T-cell lymphoma (CTCL; refs. 13, 16–18), adult T-cell lymphoma (ATL; ref. 15), anaplastic large cell lymphoma (ALCL; ref. 14), and natural killer T-cell lymphoma (NKTCL; ref. 10), as well as the B-cell lymphomas diffuse large B-cell lymphoma (DLBCL; refs. 23, 25, 26), Burkitt lymphoma (BL; refs. 21, 27, 28), and mantle cell lymphoma (MCL; refs. 22, 29). The mutational frequencies for these lymphoma types are shown in Fig. 1G and Supplementary Table S8, and additional HSTL mutation details are shown in Supplementary Table S9.

We found that mutations in *SETD2, INO80, TET3,* and *STAT5B* occurred almost exclusively in HSTLs ($P < 0.05$ in each case, Fisher exact test), compared with other T-cell and B-cell lymphoma types. On the other hand, mutations in *RHOA*, a defining feature of PTCL NOS and AITL, never occurred in HSTL cases. Additionally, HSTLs shared some mutations that have mostly been observed in B-cell lymphomas, including *PIK3CD* (23), *UBR5* (30), and *SMARCA2* (22).

These data indicate that HSTLs have a unique profile of genetic mutations that distinguishes them from other non-Hodgkin lymphoma subtypes and may underlie their distinct clinical behavior.

Functional Consequences of *SETD2* Silencing in HSTL

SETD2 was the most frequently silenced gene in HSTLs, affecting almost a third of the cases. The mutations in *SETD2* occurred predominantly in exons 3, 10–12, and 19–21 (Fig. 2A). The SET2–RPB1 interacting domain (SRI) domain (31) at the COOH-terminus of the *SETD2* protein product was the most frequently mutated protein domain, but a number of mutations were also interspersed among different domains. We noted that 67% (16/24) of the mutations in *SETD2* occurring in the 17 patients with HSTL were either frameshift or nonsense mutations. Forty-four percent (7/17) of the *SETD2*-mutated patients had more than one mutation in SETD2. We analyzed the potential biallelic nature of the *SETD2* mutations in one of these patients, by analysis of paired-end exome sequencing reads and Sanger sequencing. We found that the two *SETD2* mutations in that case occurred on mutually exclusive DNA strands, suggesting a biallelic event (Supplementary Fig. S7). Our genetic data thus indicate that *SETD2* has a tumor suppressor function in HSTLs with frequent loss-of-function mutations that may occur in biallelic fashion. No expression differences in *SETD2* were seen between wild-type and *SETD2*-mutant samples (Supplementary Fig. S8).

SETD2 functions as a methyltransferase at lysine 36 of histone 3 and 4, catalyzing H3/4K36 trimethylation at dimethyl sites. The gene has diverse functions related to cancer, including tumor proliferation, sensing and repair of DNA damage, and other oncogenic changes in gene expression (32–37). To determine the functional consequences of *SETD2* loss in HSTLs, we performed RNA interference experiments using lentiviral vectors expressing two different shRNAs targeting *SETD2* in DERL2 HSTL cells. We observed robust knockdown of *SETD2* mRNA expression in HSTL cells expressing the shRNAs targeting *SETD2* compared with nonsilencing (scramble) control (Fig. 2B). We further observed that loss of *SETD2* mRNA expression was accompanied by reduced SETD2 protein expression along with loss of H3 lysine 36 trimethylation in the same cells (H3K36me3; Fig. 2C).

We further measured the downstream effects of *SETD2* knockdown by performing RNA sequencing to define gene expression profiles of HSTL DERL2 cells with knockdown of *SETD2*. We compared the expression profiles of cells with *SETD2* knockdown through two different shRNAs and those expressing the nonsilencing control shRNA in three independent replicates (Fig. 2D). Through gene set enrichment analysis (38), we identified the pathways that were upregulated (FDR < 0.25) in the setting of reduced *SETD2* expression (Supplementary Table S10). We found that eight of the ten most significantly altered gene sets were related to proliferation or cell-cycle progression (including G_2–M checkpoint genes and core cell-cycle genes as shown in Fig. 2D), identifying proliferation as the major oncogenic process affected by *SETD2* loss in HSTL cells.

We next tested the proliferative ability of HSTL cells with intact and reduced *SETD2* expression by performing colony-forming assays in cells expressing shRNAs targeting *SETD2* as well as the nonsilencing control. We found that the cells post *SETD2* knockdown had more than 2-fold increased colony formation ($P < 0.01$, paired Wilcoxon-rank test) compared with control nonsilencing cells with intact *SETD2* expression (Fig. 2E). We also examined the effects of *SETD2* on cell proliferation using alamar blue cell quantitation assays and found that, compared with nonsilencing control (Fig. 2F), the HSTL cells expressing lower *SETD2* have significantly higher proliferation and increased cell counts ($P < 0.01$, paired Wilcoxon-rank test), consistent with its role as a tumor suppressor gene.

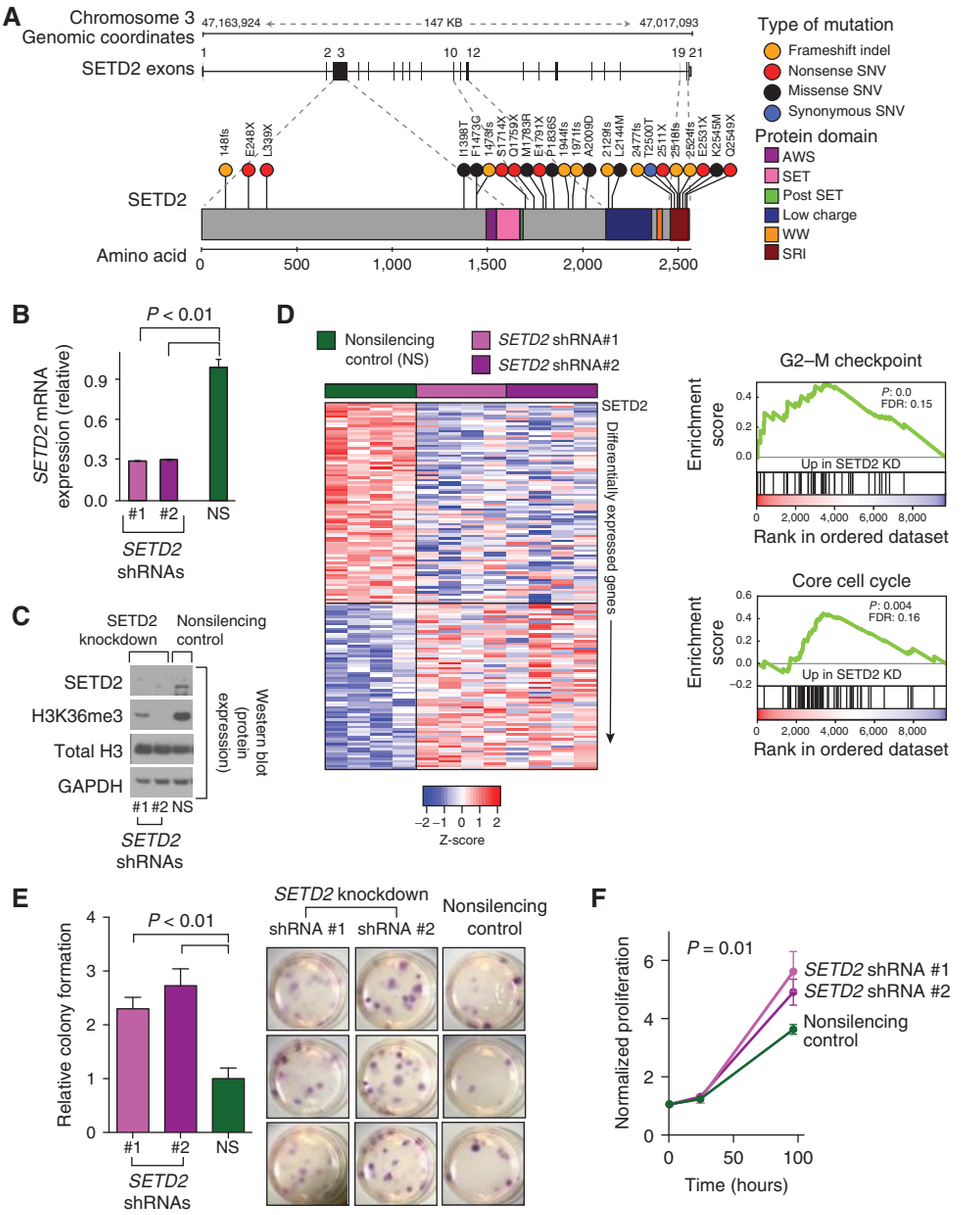

Figure 2. Discovery and characterization of HSTL *SETD2* mutations and function. **A,** Diagram of *SETD2* gene exon model, protein domains, and HSTL mutations. The exon model shows 21 exons from the canonical transcript, which spread across 147 KB of genomic space. Twenty-four *SETD2* mutations are indicated at their amino acid position, color-coded by type of mutation (yellow: frameshift; red: nonsense; black: missense; blue: synonymous). Protein domains are indicated along the gene, color-coded by domain name (purple, AWS; pink, SET; green, PostSET; blue, low charge; orange, WW; dark red, SRI). **B,** *SETD2* mRNA expression in *SETD2* shRNA knockdown and nonsilencing (NS) control in DERL2. $P < 0.01$ for both *SETD2* knockdowns versus NS control, average knockdown of >70%. **C,** Immunoblot blot showing knockdown of *SETD2* and H3K36me3 loss after *SETD2* shRNA induction in DERL2 cells. Results representative of three repeat experiments. **D,** Heat map of genes differentially expressed in DERL2 HSTL after *SETD2* knockdown compared with nonsilencing controls (left). Genes shown to have $P < 0.05$ by the Student *t* test of *SETD2* knockdown versus control. Right, Two pathways significantly upregulated in *SETD2* knockdown based on gene set enrichment analysis. Gene rank is based on *t*-statistic between control and knockdown samples. Enrichment score is shown on the y-axis as the gene list is traversed on the x-axis. **E,** Results of methylcellulose colony formation assays at 15 days of incubation compared between two cell lines expressing *SETD2* shRNA constructs (left) or NS control ($P < 0.01$ by the two-tailed Student *t* test for comparison of colony number between control and each of the two *SETD2* constructs). The right panel depicts representative MTT counterstained plates at day 15. **F,** Quantitation of *in vitro* proliferation versus time for DERL2 HSTL cells bearing *SETD2* shRNA constructs versus NS control. $P = 0.011$ by the two-tailed Student *t* test between shRNA #2 and NS control and $P = 0.0018$ between *SETD2* shRNA #1 and NS control. All error bars throughout the figure represent the standard error of the mean.

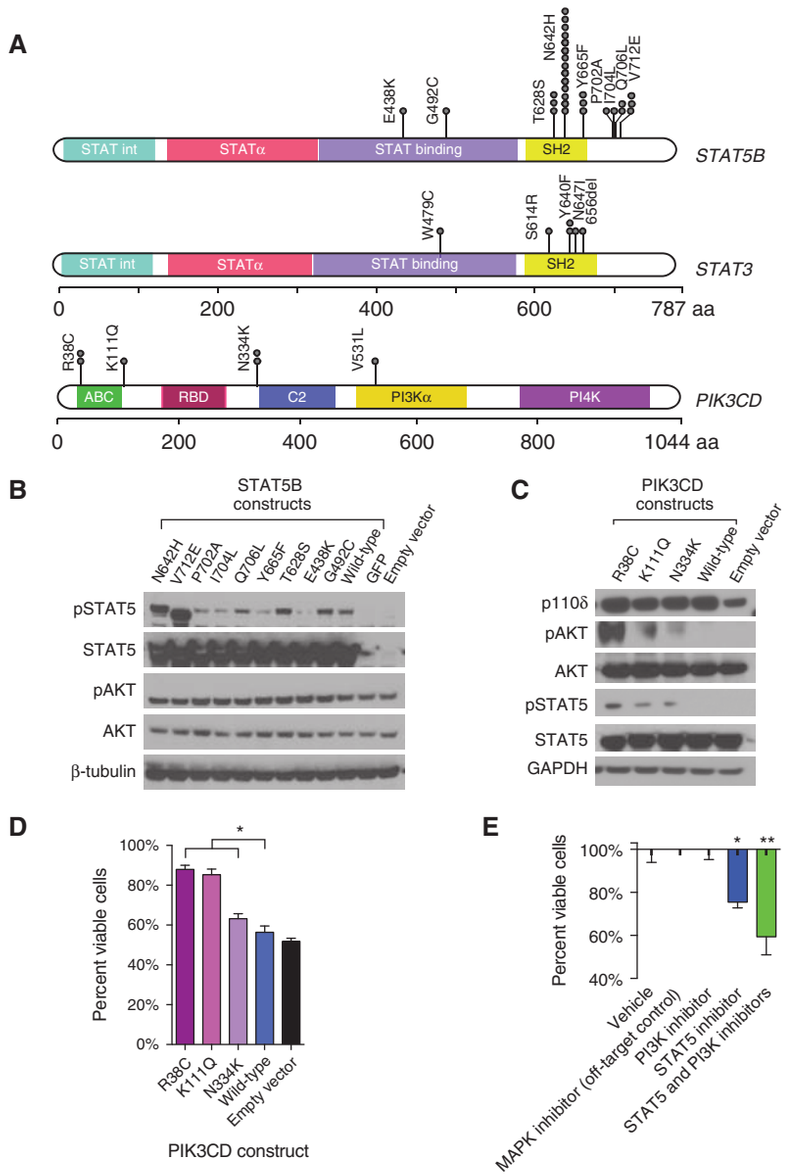

Figure 3. *STAT5B*, *STAT3*, and *PIK3CD* mutations in HSTL. **A,** Protein domains and HSTL mutations in *STAT5B, STAT3,* and *PIK3CD* in HSTL tumors are shown, with each individual mutation event denoted by a shaded circle. **B,** Immunoblots of phosphorylated and total STAT5B/AKT in 293T cells after overexpression of *STAT5B* HSTL mutant constructs (N642H, V712E, P702A, I704L, Q706L, Y665F, T628S, E438K, G492C), wild-type, or GFP-overexpression/empty-vector controls. β-Tubulin was used as a loading control. Blots are representative of three independent experiments. **C,** Immunoblots of phosphorylated and total STAT5B and AKT in DERL2 HSTL cells bearing *PIK3CD*-mutant constructs (R38C, K111Q, and N334K), wild-type *PIK3CD* retroviral expression construct, as well as empty-vector retroviral vector transfection. GAPDH was used as a loading control. Blots are representative of three independent experiments. **D,** Cell viability measurements by alamar blue fluorescence quantitation of DERL2 HSTL cells bearing mutant (R38C, K111Q, N334K) or wild-type *PIK3CD* retroviral expression constructs (as well as empty vector retroviral vector transfection). *, $P < 0.05$ for comparison between each mutant construct and wild-type control by Student *t* test. **E,** DERL2 HSTL cell viability after treatment with MEK inhibitor (selumetinib 2.5 μmol/L), PI3K inhibitor (idelalisib 10 μmol/L), STAT5B inhibitor (CAS 285986-31-4, 50 μmol/L), and vehicle control (defined as media containing the maximum concentration of DMSO as diluent from drug experiments) or STAT5B/PI3K inhibitor combination. *, $P = 0.001$ between vehicle and STAT5B inhibitor) and **, $P = 0.044$ between STAT5B inhibitor and combination inhibitor) at 96 hours of incubation. All error bars throughout the figure represent the standard error of the mean.

Our genetic and functional data thus implicate *SETD2* as a tumor suppressor gene in HSTL and demonstrate that loss-of-function *SETD2* mutations serve to increase proliferation in HSTL cells.

STAT5B, PIK3CD Mutations, and Downstream Signaling

STAT5B and *STAT3* mutations have been previously reported in HSTL (19, 20). We found somatic *STAT5B* and *STAT3* mutations occurring mostly in a mutually exclusive manner (Supplementary Fig. S9). Mutations in *STAT5B* and *STAT3* occurred predominantly in their SH2 domains, consistent with previous reports showing mutations in this gene in HSTL and other malignancies. Many of the *PIK3CD* mutations (Fig. 3A) occurred in analogous fashion to constitutively activating mutations in homologous regions of *PIK3CA*, which activates PI3K/AKT signaling in nonhematologic cancers (39).

Given this pattern of mutations, we hypothesized that *STAT5B, STAT3,* and *PIK3CD* mutations in HSTL would constitutively activate downstream signaling pathways, and that mutant STAT5B and PIK3CD may potentially cooperate to maintain proliferation pathways within HSTL cells. To test this hypothesis, we first examined the effects of the *STAT5B* mutations through their overexpression in serum-starved 293T cells (the HSTL cell line DERL2 is *STAT5B* mutant). We found that the dominant hotspot mutations N642H and V712E were particularly efficacious in maintaining STAT5 phosphorylation, as were many of the other STAT5B mutants compared with the wild-type or empty-vector control cells (Fig. 3B). Phosphorylated AKT or total AKT were not altered in these cells, indicating the *STAT5B* mutations directly enable phosphorylation of STAT5 that has been shown to have a number of downstream oncogenic effects (19).

We further investigated the impact of *PIK3CD* mutations on signaling in HSTL cells. We overexpressed three *PIK3CD*

mutants (R38C, K111Q, and N334K) found in HSTL tumors in DERL2 HSTL cells. In DERL2 cells overexpressing *PIK3CD* mutants, we found greatly increased phosphorylated AKT. In addition, we noted increased phosphorylated STAT5 compared with cells with control constructs (Fig. 3C), indicating potential cooperativity between PI3K and JAK–STAT signaling in maintaining downstream cell survival/proliferation signals.

Next, we tested the ability of PI3K mutants to protect DERL2 HSTL cells from cell death under IL2 deprivation/serum starvation conditions. After 24 hours of serum starvation and cytokine withdrawal, DERL2 cells bearing mutant *PIK3CD* constructs had significantly higher viability compared with those expressing wild-type or empty-vector controls (Fig. 3D). These data confirm that mutant *PIK3CD* could maintain cell viability and proliferation.

Finally, we tested the effects of PI3K and STAT5B signaling inhibition as a potential targeted strategy for treating HSTL. In DERL2 HSTL cells, we tested the effects of a MAPK inhibitor (selumetinib, an off-target control) as well as a STAT5B inhibitor (with CAS 285986-31-4), a PI3K inhibitor (idelalisib), and combinations of the STAT5B and PI3K inhibitors. We found that the MAPK inhibitor had no effect on cell growth, but the STAT5B inhibitor significantly attenuated cellular growth *in vitro* at 96 hours versus vehicle treatment control (Fig. 3E). Notably, the addition of PI3K inhibition to STAT5B inhibition resulted in further reduction of cellular viability than either STAT5B or PI3K inhibition alone, indicating potential synergism interaction when targeting STAT5B/PI3K cooperativity in HSTL cells.

DISCUSSION

HSTL remains among the direst cancer diagnoses any patient can face. The young age of the patients and the general lack of progress in the treatment options or outcomes further compound the grimness of the prognosis (40). A recognized risk factor for developing HSTL is the use of immune-suppressive and immune-modulatory therapies such as infliximab and azathioprine (41). The growing use of these therapies in rheumatologic and inflammatory conditions suggests that HSTL might become an increasingly larger concern in the future.

Our work indicates that the distinct clinical behavior of HSTL may originate from its distinct genetic profile. Compared with other T-cell lymphomas, the mutations in *RHOA, CD28, CCR4,* and other genes that are defining features of other T-cell lymphomas are notably absent in HSTLs. Conversely, the most frequent HSTL mutations, including *SETD2, INO80,* and *PIK3CD*, occur infrequently in other T-cell lymphomas. *STAT5B* mutations have been described in primary cutaneous γδ PTCL (19), but are not mutated in most other T-cell lymphomas derived from αβ T cells. Interestingly, *STAT3* mutations are a frequent feature of a number of lymphomas, including NKTCL (10), and diffuse large B-cell lymphoma (25).

SETD2, a histone lysine methyltransferase, was the most frequently silenced gene in HSTLs. *SETD2* has been described as a tumor suppressor gene in other malignancies, including clear cell renal carcinoma (42), DLBCL (23), and a subset of acute leukemias (43). Our genetic and experimental data identify *SETD2* as a tumor suppressor gene in HSTL. Our experiments indicate that *SETD2* mutations serve to increase proliferation in HSTL tumors. More work is needed to define the precise role of *SETD2* in HSTL oncogenesis as well as its potential role in regulating T-cell development.

The recurrent genetic mutations in HSTL also suggest new therapeutic targets in the disease with new hope for these patients. The activating mutations in *PI3KCD* and STAT signaling genes provide a framework for identifying new therapies in this disease. The rareness of the disease makes it unlikely that a comprehensive clinical trial can be performed; thus, the clinical experience with potential off-label use of these targeted therapies should be carefully reported to inform future therapies in patients with HSTL.

Thus, our data define the genetic landscape of HSTLs and implicate gene mutations linked to HSTL pathogenesis and therapeutic targets.

METHODS

Study Design and Sample Selection

HSTL tumors and normal tissues were obtained from institutions that constitute the Hematologic Malignancies Research Consortium (44) and Tenomic Consortium (45). All cases were reviewed to verify the accuracy of the pathology diagnosis. Tumor samples were derived from formalin-fixed, paraffin-embedded tissues, and normal samples were from unaffected bone marrow, when available. Archival patient tumor and normal samples, as well as clinical data, were collected according to a protocol approved by the Duke University Institutional Review Board, which was exempt from informed consent, and in accordance with the Declaration of Helsinki.

Exome Sequencing and Derivation of Genomic Data

Briefly, genomic DNA was sheared to 250 bp, and size/concentration were verified using Bioanalyzer (Agilent Technologies). Sheared DNA was end-repaired, A-tailed, and ligated to Illumina paired-end adapters. The resulting libraries were amplified using Illumina PE specific primers. Samples were column purified, and the size and quantity of the final libraries were determined using Bioanalyzer (Agilent Technologies). The resulting libraries were then hybridized for 24 hours to DNA baits provided in the SureSelect Human All Exon 50MB Kit (Agilent Technologies). The captured libraries were amplified and sequenced using the Illumina platform. FASTQs were aligned to the hg19 reference genome using BWA-MEM. Indel realignment and base quality recalibration were done with GATK tools. Variants were called using SAMtools mpileup on all samples. Somatic mutations in paired samples were called using Mutect. Variants were annotated with Annovar. Average sequencing depth throughout samples was 80×. Additional bioinformatic pipeline details as well as detailed, complete supplemental methods are in the Supplementary Methods.

Cell Lines and Cell Culture

Human embryonal kidney 293T cells were obtained from the ATCC (obtained September 2013) and maintained as a monolayer in DMEM with 10% fetal bovine serum. Modified 293T cells (GP2 cells from Clontech, obtained June 2012) were cultured in identical conditions. DERL2 and DERL7 cells (24) were obtained from Dr. Philippe Gaulard in October 2013 and subjected to exome sequencing to confirm isochromosome 7q and their other known genetic markers. Cell lines were not otherwise authenticated and assumed to be authentic as they were obtained from the original supplier. Unless otherwise noted, DERL2 and DERL7 HSTL cells were cultured in 20% human AB-positive serum in 50 ng/mL IL2 (Peprotech). For gene overexpression

experiments, serum starvation was performed by washing cells with PBS twice and then reintroducing cells to media without serum or cytokines followed by signaling or viability experiments.

Western Blotting

For each sample, 10^6 cells were washed once in ice-cold PBS and lysed in 150 microliters of RIPA buffer (Sigma) containing protease, phosphatase inhibitors (Roche), and 2 mmol/L EDTA. Crude lysates were sonicated at 10% duty cycle, intensity 4, 200 cycles/burst on a Covaris S-series device and then centrifuged at 13,000 × *g* for 10 minutes, and supernatants were used for downstream experiments. Protein (10–30 μm) was separated on 4% to 18% Bis-Tris gradient gels and transferred overnight to Immobilion PVDF membranes (Millipore) in Tris-glycine buffer with 20% methanol at 30 V. Primary antibodies (anti-SETD2, anti-H3K36me3, anti-STAT3, anti–phospho-STAT3, anti-STAT5, anti–phospho-STAT5, anti–phospho-AKT, anti-GAPDH, all from Cell Signaling Technology, and anti-p110 from Abcam) were diluted 1:1,000 in 5% BSA/TBST and bound overnight followed by washing and binding of horseradish peroxidase–conjugated anti-rabbit antibody (Santa Cruz Biotechnology). Blots were developed using SuperSignal Pico chemiluminescent substrate (Thermo Scientific).

RNA Knockdown

Lentiviral pTRIPZ constructs (Open Biosystems) containing either a scrambled nonsilencing sequence as control, or a hairpin sequence targeting the *SETD2* gene, were mixed with pVSV-G (46) and pPAX2 (Addgene #12259, from Didier Trono) and transfected into TLA-HEK-293T cells. Virus was harvested 72 hours after transfection and concentrated by centrifugation at 90,000 × *g* for 90 minutes at 4°C. DERL2 HSTL cells were infected with virus in the presence of 4 mg/mL of polybrene, using 5×10^6 cells per well in a 6-well plate by centrifugation at 1,000 × *g* for 60 minutes. Cells were selected by puromycin for 96 hours; then shRNA production was induced by doxycycline (1 g/mL replaced every 48 hours) for 96 hours prior to downstream experimentation. Successful knockdown of *SETD2* was confirmed by quantitative PCR (qPCR) and Western blot. RNA-sequencing methods and derivation of gene expression profiles of HSTL cells with SETD2 or control shRNAs is described in the Supplementary Methods.

Lentiviral Gene Overexpression

mRNA from DERL2 HSTL cells was extracted, and a corresponding cDNA library was used to amplify full-length PIK3CD and STAT5B sequences which were ligated downstream of the CMV promoter at the PacI restriction site of the pQCXIP retroviral vector using PacI restriction sites on the flanking cloning primer used for gene amplication. cDNA constructs in pQCXIP plasmids were verified using Sanger sequencing, and mutagenesis to yield desired mutant constructs was performed by PCR technique using the New England Biolabs mutagenesis kit. Mutant cDNA expression clones were again verified by Sanger sequencing. Lentiviral particles were produced via pQCXIP cotransfection with VSV-G plasmid in GP2 293 cells, and virus was harvested and cells transfected as described above for lentiviral shRNA constructs.

Colony-Forming Assays

DERL2 HSTL cells, exposed to doxycycline for >96 hours, were plated in 1,000/mL in Iscove's Modified Dulbecco's Medium–based methylcellulose semisolid media containing 50 ng/ML IL2, 25 ng/mL stem cell factor (SCF) and 1 mg/mL doxycycline. Cells were cultured for 4 weeks at 37°C and 5% CO_2. Ten percent of media volume containing 10× concentrations of IL2, SCF, and doxycycline were added every 5 days. Once visible colonies formed, plates were photographed, and colonies were identified and counted.

Cellular Proliferation Assays

To measure cellular proliferation over time, cells were plated in 96-well plates, 5,000 cells/well, in 220 μL of media in replicates with conditions varied according to the experimental design. Quantitation of the number of cells at each desired time point was accomplished by measured by adding 25 μL alamar blue to replicate wells and measuring fluorescence (excitation 430 nmol/L, emission 490 nmol/L) on a Tecan plate reader after 6-hour incubation of alamar blue with cells. Fluorescence values obtained in this manner were normalized to values obtained by adding alamar blue at time = 0 or at the commencement of the experiment in order to obtain values relative to proliferation over time.

Pharmacologic Treatment of Cell Lines

The viability of DERL2 HSTL cells exposed to small-molecule inhibitors was performed as previously described (47), with the exception that alamar blue fluorescence was measured instead of absorbance values post MTT and detergent incubation. Selumetinib was obtained from Selleck Chemicals, STAT5B inhibitor (CAS 285986-31-4) was obtained from Millipore, and idelalisib was obtained from Gilead biosciences. Controls included carrier control and 10% DMSO control for 100% and 0% proliferation controls, respectively. After 3 days of incubation, 25 μL of alamar blue reagent was added to the cells, which were then incubated at 37°C for 12 hours. Fluorescence values at 590 nm were assessed with a plate reader device (Tecan). Normalized proliferation (% viable cells) for each well was calculated as: Normalized proliferation = (well absorbance – 10% DMSO control absorbance)/(carrier control absorbance – 10% DMSO control) or values were normalized to fluorescence values at baseline for cell line or drug assay experiments.

Statistical Analysis

The Fisher exact test was used to compare mutation frequencies between lymphoma types and between subgroups of HSTL. The Cox proportional hazards model was used to test significance in survival associations with clinical and molecular covariates. Survival curves were drawn using the Kaplan–Meier method. Individual methods used for analysis of clinical, pathologic, and mutational features and survival are listed in the Supplementary Methods.

Data Availability

Primary sequence data are available at the European Genome-phenome Archive (EGA) under accession number EGAS00001002182.

Disclosure of Potential Conflicts of Interest

E.D. Hsi is a consultant/advisory board member for Seattle Genetics. C.R. Flowers reports receiving commercial research grants from AbbVie, Acerta Pharma, Roche/Genentech, Gilead, Infinity Pharmaceuticals, Millennium Pharmaceuticals, Inc./Takeda, and TG Therapeutics, and is a consultant/advisory board member for Hoffmann-La Roche/Genentech, Gilead, and Bayer. R.D. Gascoyne has received speakers bureau honoraria from Seattle Genetics. S.S. Davé reports receiving a commercial research grant from Janssen. No potential conflicts of interest were disclosed by the other authors.

Authors' Contributions

Conception and design: M. McKinney, P. Gaulard, J. Iqbal, S.S. Davé
Development of methodology: M. McKinney, A.B. Moffitt, N.S. Davis, J. Zhang, A. Reddy, S.S. Davé
Acquisition of data (provided animals, acquired and managed patients, provided facilities, etc.): M. McKinney, P. Gaulard, M. Travert, L. De Leval, A. Nicolae, M. Raffeld, E.S. Jaffe, S. Pittaluga, L. Xi, T. Heavican, J. Iqbal, K. Belhadj, M.H. Delfau-Larue, M.B. Czader, I.S. Lossos, J.R. Chapman-Fredricks, K.L. Richards, Y. Fedoriw,

S.L. Ondrejka, E.D. Hsi, L. Low, D. Weisenurger, W.C. Chan, N. Mehta-Shah, S. Horwitz, L. Bernal-Mizrachi, C.R. Flowers, A.W. Beaven, L. Baseggio, M. Parrens, A. Moreau, P. Sujobert, M. Pilichowska, A. Chadburn, R.K.H. Au-Yeung, G. Srivastava, W.W.L. Choi, I. Aurer, S. Basic-Kinda, R.D. Gascoyne, N.S. Davis, C. Love, S. Levy, Y. Zhuang, S.S. Davé

Analysis and interpretation of data (e.g., statistical analysis, biostatistics, computational analysis): M. McKinney, A.B. Moffitt, T. Heavican, J. Iqbal, I.S. Lossos, J.R. Chapman-Fredricks, C.R. Flowers, A.M. Evens, I. Aurer, J. Zhang, D. Rajagopalan, A. Reddy, J. Datta, D.B. Dunson, S.S. Davé

Writing, review, and/or revision of the manuscript: M. McKinney, A.B. Moffitt, P. Gaulard, L. De Leval, M. Raffeld, L. Xi, J. Iqbal, M.B. Czader, I.S. Lossos, J.R. Chapman-Fredricks, K.L. Richards, Y. Fedoriw, S.L. Ondrejka, E.D. Hsi, D. Weisenburger, W.C. Chan, N. Mehta-Shah, S. Horwitz, L. Bernal-Mizrachi, C.R. Flowers, A.W. Beaven, M. Parihar, L. Baseggio, M. Pilichowska, A.M. Evens, A. Chadburn, J.R. Goodlad, I. Aurer, R.D. Gascoyne, S.S. Davé

Administrative, technical, or material support (i.e., reporting or organizing data, constructing databases): M. McKinney, V. Fataccioli, M. Parihar, A.M. Evens, G. Li, J. Zhang, C. Love, S. Levy, S.S. Davé

Study supervision: M. McKinney, L. Bernal-Mizrachi, S.S. Davé

Grant Support

This work was supported by Janssen and by grants from the NIH (CA195173 and CA136895). M. McKinney was supported by the Lymphoma Research Foundation. A.B. Moffitt was supported by the Hertz Foundation Fellowship and the National Science Foundation Graduate Research Fellowship.

The costs of publication of this article were defrayed in part by the payment of page charges. This article must therefore be hereby marked *advertisement* in accordance with 18 U.S.C. Section 1734 solely to indicate this fact.

Received March 23, 2016; revised January 13, 2017; accepted January 23, 2017; published OnlineFirst January 25, 2017.

REFERENCES

1. Belhadj K, Reyes F, Farcet J-P, Tilly H, Bastard C, Angonin R, et al. Hepatosplenic γδ T-cell lymphoma is a rare clinicopathologic entity with poor outcome: report on a series of 21 patients. Blood 2003;102:4261–9.
2. Weisenburger DD, Savage KJ, Harris NL, Gascoyne RD, Jaffe ES, MacLennan KA, et al. Peripheral T-cell lymphoma, not otherwise specified: a report of 340 cases from the International Peripheral T-cell Lymphoma Project. Blood 2011;117:3402–8.
3. Alonsozana E, Stamberg J, Kumar D, Jaffe E, Medeiros L, Frantz C, et al. Isochromosome 7q: the primary cytogenetic abnormality in hepatosplenic T cell lymphoma. Leukemia 1997;11:1367–72.
4. Wlodarska I, Martin-Garcia N, Achten R, De Wolf-Peeters C, Pauwels P, Tulliez M, et al. Fluorescence in situ hybridization study of chromosome 7 aberrations in hepatosplenic T-cell lymphoma: isochromosome 7q as a common abnormality accumulating in forms with features of cytologic progression. Genes Chromosomes Cancer 2002;33:243–51.
5. Finalet Ferreiro J, Rouhigharabaei L, Urbankova H, van der Krogt JA, Michaux L, Shetty S, et al. Integrative genomic and transcriptomic analysis identified candidate genes implicated in the pathogenesis of hepatosplenic T-cell lymphoma. PloS ONE 2014;9:e102977.
6. Travert M, Huang Y, de Leval L, Martin-Garcia N, Delfau-Larue MH, Berger F, et al. Molecular features of hepatosplenic T-cell lymphoma unravels potential novel therapeutic targets. Blood 2012;119:5795–806.
7. Cools J. RHOA mutations in peripheral T cell lymphoma. Nat Genet 2014;46:320–1.
8. Palomero T, Couronné L, Khiabanian H, Kim M-Y, Ambesi-Impiombato A, Perez-Garcia A, et al. Recurrent mutations in epigenetic regulators, RHOA and FYN kinase in peripheral T cell lymphomas. Nat Genet 2014;46:166–70.
9. Sakata-Yanagimoto M, Enami T, Yoshida K, Shiraishi Y, Ishii R, Miyake Y, et al. Somatic RHOA mutation in angioimmunoblastic T cell lymphoma. Nat Genet 2014;46:171–5.
10. Jiang L, Gu ZH, Yan ZX, Zhao X, Xie YY, Zhang ZG, et al. Exome sequencing identifies somatic mutations of DDX3X in natural killer/T-cell lymphoma. Nat Genet 2015;47:1061–6.
11. Odejide O, Weigert O, Lane AA, Toscano D, Lunning MA, Kopp N, et al. A targeted mutational landscape of angioimmunoblastic T-cell lymphoma. Blood 2014;123:1293–6.
12. Yoo HY, Sung MK, Lee SH, Kim S, Lee H, Park S, et al. A recurrent inactivating mutation in RHOA GTPase in angioimmunoblastic T cell lymphoma. Nat Genet 2014;46:371–5.
13. Choi J, Goh G, Walradt T, Hong BS, Bunick CG, Chen K, et al. Genomic landscape of cutaneous T cell lymphoma. Nat Genet 2015;47:1011–9.
14. Crescenzo R, Abate F, Lasorsa E, Gaudiano M, Chiesa N, Di Giacomo F, et al. Convergent mutations and kinase fusions lead to oncogenic STAT3 activation in anaplastic large cell lymphoma. Cancer Cell 2015;27:516–32.
15. Kataoka K, Nagata Y, Kitanaka A, Shiraishi Y, Shimamura T, Yasunaga J-i, et al. Integrated molecular analysis of adult T cell leukemia/lymphoma. Nat Genet 2015;47:1304–15.
16. Ungewickell A, Bhaduri A, Rios E, Reuter J, Lee CS, Mah A, et al. Genomic analysis of mycosis fungoides and Sezary syndrome identifies recurrent alterations in TNFR2. Nat Genet 2015;47:1056–60.
17. Wang L, Ni X, Covington KR, Yang BY, Shiu J, Zhang X, et al. Genomic profiling of Sezary syndrome identifies alterations of key T cell signaling and differentiation genes. Nat Genet 2015;47:1426–34.
18. da Silva Almeida A, Abate F, Khiabanian H, Martinez-Escala E, Guitart J, Tensen C, et al. The mutational landscape of cutaneous T cell lymphoma and Sezary syndrome. Nat Genet 2015;47:1465–70.
19. Küçük C, Jiang B, Hu X, Zhang W, Chan JKC, Xiao W, et al. Activating mutations of STAT5B and STAT3 in lymphomas derived from γδ-T or NK cells. Nat Commun 2015;6:6025.
20. Nicolae A, Xi L, Pittaluga S, Abdullaev Z, Pack S, Chen J, et al. Frequent STAT5B mutations in γδ hepatosplenic T-cell lymphomas. Leukemia 2014;28:2244–8.
21. Love C, Sun Z, Jima D, Li G, Zhang J, Miles R, et al. The genetic landscape of mutations in Burkitt lymphoma. Nat Genet 2012;44:1321–5.
22. Zhang J, Jima D, Moffitt AB, Liu Q, Czader M, Hsi ED, et al. The genomic landscape of mantle cell lymphoma is related to the epigenetically determined chromatin state of normal B cells. Blood 2014;123:2988–96.
23. Zhang J, Grubor V, Love CL, Banerjee A, Richards KL, Mieczkowski PA, et al. Genetic heterogeneity of diffuse large B-cell lymphoma. Proc Natl Acad Sci 2013;110:1398–403.
24. Di Noto R, Pane F, Camera A, Luciano L, Barone M, Pardo CL, et al. Characterization of two novel cell lines, DERL-2 ($CD56^+/CD3^+/TCR\gamma\delta^+$) and DERL-7 ($CD56^+/CD3^-/TCR\gamma\delta^-$), derived from a single patient with $CD56^+$. Leukemia 2001;15:1641–9.
25. Morin RD, Mendez-Lago M, Mungall AJ, Goya R, Mungall KL, Corbett RD, et al. Frequent mutation of histone-modifying genes in non-Hodgkin lymphoma. Nature 2011;476:298–303.
26. Lohr JG, Stojanov P, Lawrence MS, Auclair D, Chapuy B, Sougnez C, et al. Discovery and prioritization of somatic mutations in diffuse large B-cell lymphoma (DLBCL) by whole-exome sequencing. Proc Natl Acad Sci U S A 2012;109:3879–84.
27. Schmitz R, Young RM, Ceribelli M, Jhavar S, Xiao W, Zhang M, et al. Burkitt lymphoma pathogenesis and therapeutic targets from structural and functional genomics. Nature 2012;490:116–20.
28. Richter J, Schlesner M, Hoffmann S, Kreuz M, Leich E, Burkhardt B, et al. Recurrent mutation of the ID3 gene in Burkitt lymphoma identified by integrated genome, exome and transcriptome sequencing. Nat Genet 2012;44:1316–20.
29. Beà S, Valdés-Mas R, Navarro A, Salaverria I, Martín-Garcia D, Jares P, et al. Landscape of somatic mutations and clonal evolution in mantle cell lymphoma. Proc Natl Acad Sci 2013;110:18250–5.

30. Meissner B, Kridel R, Lim RS, Rogic S, Tse K, Scott DW, et al. The E3 ubiquitin ligase UBR5 is recurrently mutated in mantle cell lymphoma. Blood 2013;121:3161–4.
31. Rebehmed J, Revy P, Faure G, de Villartay JP, Callebaut I. Expanding the SRI domain family: a common scaffold for binding the phosphorylated C-terminal domain of RNA polymerase II. FEBS Lett 2014;588:4431–7.
32. Edmunds JW, Mahadevan LC, Clayton AL. Dynamic histone H3 methylation during gene induction: HYPB/Setd2 mediates all H3K36 trimethylation. EMBO J 2008;27:406–20.
33. Xie P, Tian C, An L, Nie J, Lu K, Xing G, et al. Histone methyltransferase protein SETD2 interacts with p53 and selectively regulates its downstream genes. Cell Signal 2008;20:1671–8.
34. Yoh SM, Lucas JS, Jones KA. The Iws1:Spt6:CTD complex controls cotranscriptional mRNA biosynthesis and HYPB/Setd2-mediated histone H3K36 methylation. Genes Dev 2008;22:3422–34.
35. Li F, Mao G, Tong D, Huang J, Gu L, Yang W, et al. The histone mark H3K36me3 regulates human DNA mismatch repair through its interaction with MutSalpha. Cell 2013;153:590–600.
36. Carvalho S, Vitor AC, Sridhara SC, Martins FB, Raposo AC, Desterro JM, et al. SETD2 is required for DNA double-strand break repair and activation of the p53-mediated checkpoint. eLife 2014;3:e02482.
37. Pfister SX, Ahrabi S, Zalmas LP, Sarkar S, Aymard F, Bachrati CZ, et al. SETD2-dependent histone H3K36 trimethylation is required for homologous recombination repair and genome stability. Cell Rep 2014;7:2006–18.
38. Subramanian A, Tamayo P, Mootha VK, Mukherjee S, Ebert BL, Gillette MA, et al. Gene set enrichment analysis: a knowledge-based approach for interpreting genome-wide expression profiles. Proc Natl Acad Sci U S A 2005;102:15545–50.
39. Samuels Y, Wang Z, Bardelli A, Silliman N, Ptak J, Szabo S, et al. High frequency of mutations of the PIK3CA gene in human cancers. Science 2004;304:554.
40. Farcet JP, Gaulard P, Marolleau JP, Le Couedic JP, Henni T, Gourdin MF, et al. Hepatosplenic T-cell lymphoma: sinusal/sinusoidal localization of malignant cells expressing the T-cell receptor gamma delta. Blood 1990;75:2213–9.
41. Mackey AC, Green L, Liang LC, Dinndorf P, Avigan M. Hepatosplenic T cell lymphoma associated with infliximab use in young patients treated for inflammatory bowel disease. J Pediatr Gastroenterol Nutr 2007;44:265–7.
42. Dalgliesh GL, Furge K, Greenman C, Chen L, Bignell G, Butler A, et al. Systematic sequencing of renal carcinoma reveals inactivation of histone modifying genes. Nature 2010;463:360–3.
43. Zhu X, He F, Zeng H, Ling S, Chen A, Wang Y, et al. Identification of functional cooperative mutations of SETD2 in human acute leukemia. Nat Genet 2014;46:287–93.
44. Jima DD, Zhang J, Jacobs C, Richards KL, Dunphy CH, Choi WW, et al. Deep sequencing of the small RNA transcriptome of normal and malignant human B cells identifies hundreds of novel microRNAs. Blood 2010;116:e118–27.
45. de Leval L, Parrens M, Le Bras F, Jais J-P, Fataccioli V, Martin A, et al. Angioimmunoblastic T-cell lymphoma is the most common T-cell lymphoma in two distinct French information data sets. Haematologica 2015;100:e361–e4.
46. Stewart SA, Dykxhoorn DM, Palliser D, Mizuno H, Yu EY, An DS, et al. Lentivirus-delivered stable gene silencing by RNAi in primary cells. RNA (New York, NY) 2003;9:493–501.
47. Walsh K, McKinney MS, Love C, Liu Q, Fan A, Patel A, et al. PAK1 mediates resistance to PI3K inhibition in lymphomas. Clin Cancer Res 2013;19:1106–15.